Cell Reports

The histone chaperone FACT facilitates heterochromatin spreading by regulating histone turnover and H3K9 methylation states

Graphical abstract

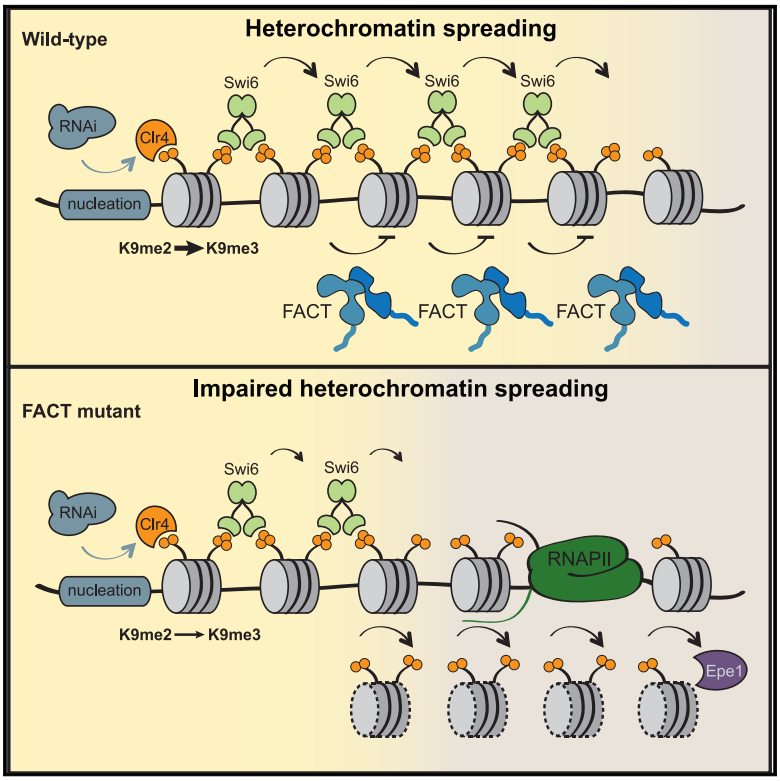

Highlights

- FACT facilitates heterochromatin spreading in fission yeast
- FACT promotes the transition of H3K9me2 to H3K9me3 by the methyltransferase Clr4
- FACT suppresses heterochromatic histone turnover
- The jumonji protein Epe1 counteracts FACT-mediated spreading

Authors

Magdalena Murawska, R.A. Greenstein, Tamas Schauer, ..., Andreas G. Ladurner, Bassem Al-Sady, Sigurd Braun

Correspondence

magdalena.murawska@bmc.med.lmu.de (M.M.), bassem.al-sady@ucsf.edu (B.A.-S.), sigurd.braun@gen.bio.uni-giessen.de (S.B.)

In brief

Heterochromatin establishment requires distinct nucleation and spreading steps. Murawska et al. show that the conserved and essential histone chaperone FACT facilitates the heterochromatin spreading process by maintaining low heterochromatic histone turnover, which enables a productive H3K9 trimethylation step by the methyltransferase Clr4 in fission yeast.

Murawska et al., 2021, Cell Reports *37*, 109944
November 2, 2021
https://doi.org/10.1016/j.celrep.2021.109944

Cell Reports

CellPress
OPEN ACCESS

Report

The histone chaperone FACT facilitates heterochromatin spreading by regulating histone turnover and H3K9 methylation states

Magdalena Murawska,[1,*] R.A. Greenstein,[2,3,4] Tamas Schauer,[5] Karl C.F. Olsen,[1,6] Henry Ng,[2,3,4] Andreas G. Ladurner,[1,6] Bassem Al-Sady,[2,3,*] and Sigurd Braun[1,6,7,8,*]

[1]Physiological Chemistry, Biomedical Center, Faculty of Medicine, Ludwig-Maximilians-University Munich, 82152 Planegg-Martinsried, Germany
[2]Department of Microbiology and Immunology, University of California, San Francisco, CA 94143, USA
[3]George Williams Hooper Research Foundation, University of California, San Francisco, CA 94143, USA
[4]TETRAD Graduate Program, University of California, San Francisco, CA 94143, USA
[5]Bioinformatics Unit, Biomedical Center, Faculty of Medicine, Ludwig-Maximilians-University Munich, 82152 Planegg-Martinsried, Germany
[6]International Max Planck Research School for Molecular and Cellular Life Sciences, 82152 Planegg-Martinsried, Germany
[7]Institute for Genetics, Justus-Liebig University Giessen, 35392 Giessen, Germany
[8]Lead contact
*Correspondence: magdalena.murawska@bmc.med.lmu.de (M.M.), bassem.al-sady@ucsf.edu (B.A.-S.), sigurd.braun@gen.bio.uni-giessen.de (S.B.)
https://doi.org/10.1016/j.celrep.2021.109944

SUMMARY

Heterochromatin formation requires three distinct steps: nucleation, self-propagation (spreading) along the chromosome, and faithful maintenance after each replication cycle. Impeding any of those steps induces heterochromatin defects and improper gene expression. The essential histone chaperone FACT (facilitates chromatin transcription) has been implicated in heterochromatin silencing, but the mechanisms by which FACT engages in this process remain opaque. Here, we pinpoint its function to the heterochromatin spreading process in fission yeast. FACT impairment reduces nucleation-distal H3K9me3 and HP1/Swi6 accumulation at subtelomeres and derepresses genes in the vicinity of heterochromatin boundaries. FACT promotes spreading by repressing heterochromatic histone turnover, which is crucial for the H3K9me2 to me3 transition that enables spreading. FACT mutant spreading defects are suppressed by removal of the H3K9 methylation antagonist Epe1. Together, our study identifies FACT as a histone chaperone that promotes heterochromatin spreading and lends support to the model that regulated histone turnover controls the propagation of repressive methylation marks.

INTRODUCTION

The eukaryotic genome is partitioned into transcriptionally active euchromatin and transcriptionally silent heterochromatin. Heterochromatin is instrumental for genome protection, proper chromosome segregation, and cell fate maintenance (Becker et al., 2016; Janssen et al., 2018; Penagos-Puig and Furlan-Magaril, 2020).

Fission yeast (*Schizosaccharomyces pombe*) is a powerful model organism to study heterochromatin formation and inheritance (Allshire and Ekwall, 2015; Goto and Nakayama, 2012; Mizuguchi et al., 2015). *S. pombe* heterochromatin is present at distinct chromosomal regions, such as repetitive sequences at pericentromeres, subtelomeres, and the silent mating-type locus, and is characterized by the presence of hypoacetylated and H3K9-methylated nucleosomes, which are bound by the HP1 family chromodomain proteins Swi6 and Chp2 (Allshire and Ekwall, 2015). This heterochromatin platform recruits further factors to safeguard transcriptional and post-transcriptional gene silencing (Ekwall et al., 1995; Reyes-Turcu and Grewal, 2012; Yamada et al., 2005).

Heterochromatin assembly initiates at nucleation sites where the RNAi machinery, cis-DNA sequences, or the shelterin complex recruit the sole H3K9 methyltransferase, Clr4 (Martienssen and Moazed, 2015; van Emden et al., 2019; Wang and Moazed, 2017; Wang et al., 2016). While Clr4 modifies H3K9, it also binds the K9 methylation mark through its chromodomain. This allows for a "write" and "read" mechanism of self-propagation of H3K9me and its re-establishment after each cell division (Chen et al., 2008; Zhang et al., 2008). Differential affinity of Clr4 and Swi6 chromodomains toward H3K9me2 and H3K9me3, respectively, is believed to be important for efficient heterochromatin spreading from nucleation sites (Al-Sady et al., 2013; Jih et al., 2017; Zhang et al., 2008). While nucleation of heterochromatin has been extensively studied, the mechanisms of its expansion remain obscure.

The histone chaperone FACT (facilitates chromatin transcription) is an essential and highly conserved dimer composed of

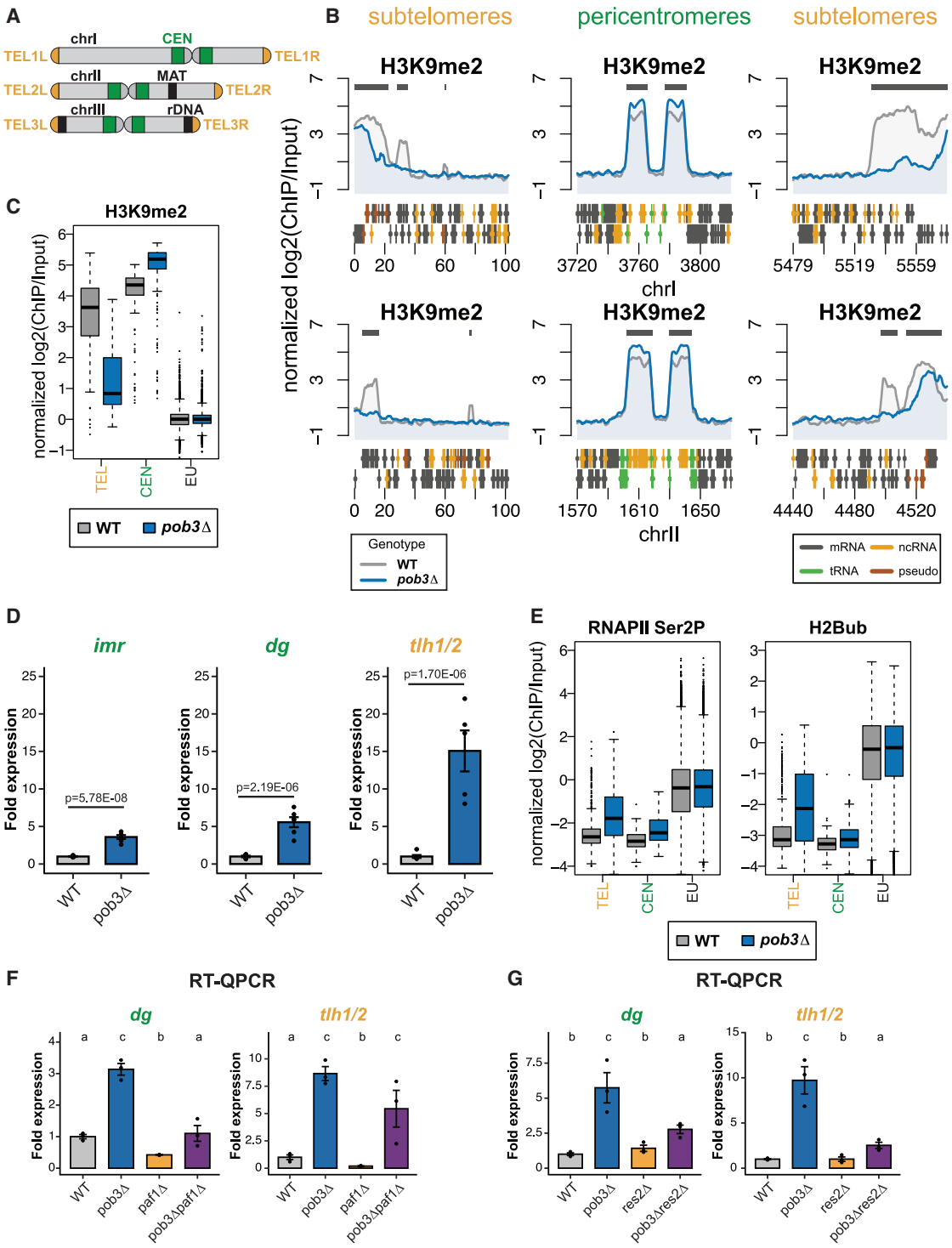

Figure 1. Transcriptional silencing is impaired in the FACT mutant

(A) *Schizosaccharomyces pombe* chromosomes with indicated heterochromatin loci. CEN, pericentromere; MAT, mating-type locus; rDNA, ribosomal DNA; TEL, subtelomere.

(B) H3K9me2 ChIP-seq enrichment [normalized log2(ChIP/Input)] at subtelomeres and pericentromeres in WT and *pob3Δ* on chromosomes I and II. Gray indicates WT, and blue indicates *pob3Δ*. Both (+) and (−) DNA strands are shown with gene coding (mRNA), noncoding (ncRNA), tRNA, and pseudogenes. Dark gray bars over the graphs point to the localization of H3K9me2 in the WT strain.

(legend continued on next page)

Spt16 and Pob3/SSRP1. FACT facilitates nucleosome disassembly and reassembly in the wake of RNA polymerase II (RNAPII) passage at transcribed genes (Duina et al., 2007; Formosa and Winston, 2020; Lee et al., 2017; Murawska et al., 2020; Orphanides et al., 1998). In addition, FACT is implicated in numerous chromatin-associated processes, such as DNA repair and replication (Herrera-Moyano et al., 2014) or higher-order chromatin formation (Garcia-Luis et al., 2019; Murawska et al., 2020).

We showed previously that FACT is also involved in pericentromeric heterochromatin silencing, acting in a pathway independent of the RNAi machinery (Lejeune et al., 2007). A recent study further showed that FACT interacts with a perinuclear complex that facilitates FACT loading on the mating-type locus to suppress histone turnover and promote heterochromatin maintenance (Holla et al., 2020). However, the exact function of FACT in heterochromatin formation needs to be established. Specifically, whether FACT acts during heterochromatin nucleation, spreading, and/or maintenance phases remains unknown.

Here, we demonstrate that transcriptional silencing is impaired throughout heterochromatin in mutants deficient in FACT but the heterochromatin structure is particularly affected at heterochromatin-euchromatin transitions. We provide further evidence that FACT limits heterochromatic histone turnover, which is critical for a productive K9 trimethylation step by Clr4. Deletion of the jumonji protein Epe1 specifically suppresses the spreading defects of FACT by reducing heterochromatic histone turnover and transcription. Together, our data reveal an unexpected function of FACT in heterochromatin spreading along chromosomal arms.

RESULTS

Transcriptional gene silencing is impaired at different levels at pericentromeres and subtelomeres in the FACT mutant

In order to understand the functional contribution of FACT to heterochromatin silencing, we systematically analyzed the heterochromatin structure at the genome-wide level in *S. pombe* (Figure 1A). We utilized the *pob3Δ* mutant, which in contrast to other model organisms is not lethal but recapitulates many known FACT defects (Murawska et al., 2020). In agreement with previous studies, chromatin immunoprecipitation sequencing (ChIP-seq) revealed only a subtle change of H3K9me2 at pericentromeres (Figures 1B, 1C, and S1D) (Holla et al., 2020; Lejeune et al., 2007). This result suggests that heterochromatin domains strictly depending on RNAi are not impaired when FACT is depleted. In contrast, there was a substantial reduction of H3K9me2 at the mating-type locus, in agreement with a previous study (Holla et al., 2020) (Figure S1A), and at the subtelomeres (Figure 1B). Interestingly, H3K9me2 was more affected at the distal subtelomeric heterochromatin than at the telomeric ends where heterochromatin nucleation takes place. Moreover, rDNA and several facultative heterochromatin islands also had reduced H3K9me2 levels in *pob3Δ* (Figures S1B and S1C).

Next, we analyzed whether changes in H3K9me2 are accompanied by the derepression of heterochromatic transcripts in *pob3Δ*. RT-qPCR analysis showed a substantial accumulation of subtelomeric transcripts but only a small increase in pericentromeric RNAs (Figure 1D). The absence of strong pericentromeric defects suggested a role of FACT in transcriptional gene silencing (TGS) rather than post-TGS. Hence, we analyzed the abundance of the transcription machinery at heterochromatin in *pob3Δ* using previously published ChIP-seq datasets (Murawska et al., 2020). At subtelomeres, but not at euchromatin, we found increased signals of elongating RNAPII (RNAPII Ser2P) and H2B ubiquitination (H2Bub), a histone mark associated with active transcription (Figures 1E and S1D). RNAPII Ser2P and H2Bub were also slightly enriched at pericentromeres, in agreement with our expression analysis (Figure 1E). Moreover, deletion of factors involved in transcription elongation (*paf1+*) or termination (*res2+*) alleviated the silencing defects in *pob3Δ* (Figures 1F and 1G). Together, our data suggest that TGS is impaired at the genome-wide scale in *pob3Δ* and sites distal to heterochromatin nucleation sites are most vulnerable to FACT depletion.

To gain a more comprehensive picture of FACT engagement with heterochromatin, we examined the genome-wide distribution of Pob3 and Spt16 (Figure S1E). This analysis showed the highest levels of FACT at euchromatin, lower levels at subtelomeres, and the lowest levels at pericentromeres. This is in accordance with recent models supporting enhanced FACT recruitment via distorted nucleosomes, such as at transcribed regions (Liu et al., 2020). Further, we showed that FACT accumulates at the core centromeres, which are transcribed but largely void of H3K9me2 (Figure S1F) (Sadeghi et al., 2014). Thus, we conclude that FACT accumulates only at relatively low levels at silent regions, which is likely sufficient to maintain heterochromatin functions.

Altogether, our genome-wide analysis suggests that FACT's contribution to heterochromatin maintenance is less critical at regions containing frequent nucleation sites. However, its role becomes more important at nucleation-distal regions.

FACT facilitates heterochromatin spreading

Although H3K9me2 was reduced at subtelomeres in the *pob3Δ* strain, we found that Clr4 binding was unaltered (Figure S2A).

(C) Box plot of H3K9me2 ChIP-seq enrichment [normalized log2(ChIP/Input)] calculated in 250-bp bins in WT and *pob3Δ*. The average of two biological replicates is shown. EU, rest of the genome (euchromatin).
(D) RT-qPCR analysis. Expression of pericentromeric (*imr*, *dg*) and subtelomeric (*tlh1/2*) transcripts in *pob3Δ* relative to WT after normalization to *act1+*. n = 5 to 6 biological replicates. Data are presented as the mean ± SEM. Statistical analysis (one-way ANOVA) was done on log2-transformed values.
(E) Box plots of RNAPII Ser2P and H2Bub ChIP-seq enrichment [normalized log2(ChIP/Input)] calculated in 250-bp bins in WT and *pob3Δ*. The average of two biological replicates is shown. Labeling as in (C).
(F and G) RT-qPCR analysis. Expression of heterochromatin transcripts in *pob3Δ*, *paf1Δ*, and *pob3Δpaf1Δ* (F) or *pob3Δ*, *res2Δ*, and *pob3Δres2Δ* (G) relative to WT after normalization to *act1+*. n = 3 biological replicates. Data are presented as the mean ± SEM. Statistical analysis performed as in (D). Different letters denote significant differences with a Tukey post hoc test at $p < 0.05$.
See also Figure S1 and Table S3.

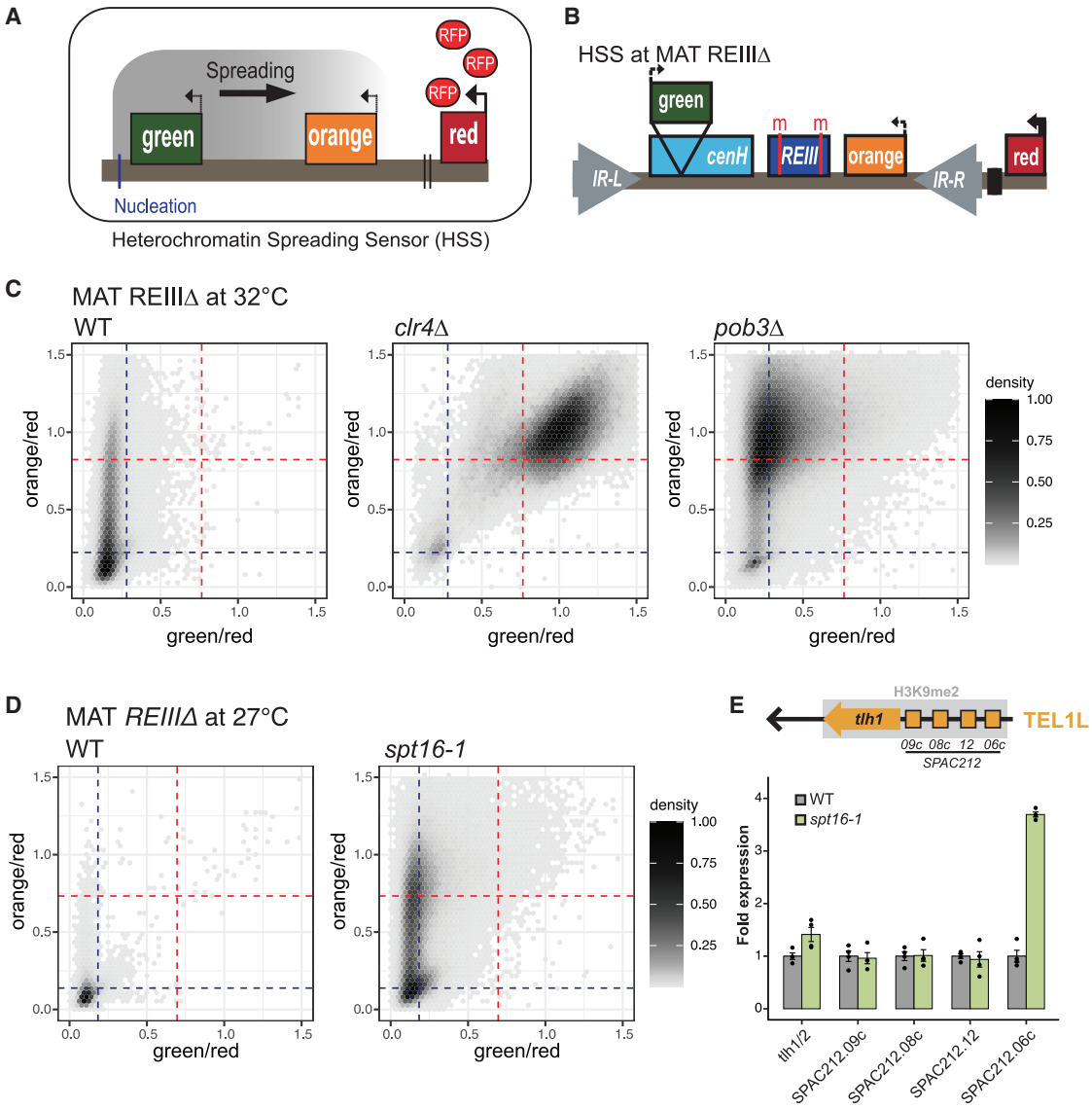

Figure 2. FACT mutants have heterochromatin spreading defects at engineered and endogenous heterochromatin

(A) Heterochromatin spreading sensor (HSS) scheme.

(B) REIIIΔ reporter scheme. Red bars and red "m" letters denote mutation of the Aft1/Pcr1 binding sites.

(C) Two-dimensional-density hexbin plot showing the red-normalized green and orange fluorescence for WT, *clr4Δ*, and *pob3Δ* MAT_REIIIΔ cells grown at 32°C. A density bar represents the fraction of the most dense bin. Threshold values for the fully expressed state ("on") and fully repressed state ("off") in each color are indicated by red and blue guide lines, respectively. One (WT, *clr4Δ*) or four (*pob3Δ*) independent isolates were analyzed and are shown in a combined plot.

(D) Two-dimensional-density hexbin plot showing the red-normalized green and orange fluorescence for WT and *spt16-1* MAT_REIIIΔ cells grown at 27°C. One (WT) or four (*spt16-1*) independent isolates were analyzed and are shown in a combined plot. Labeling as in (C).

(E) RT-qPCR analysis. Expression of transcripts at TEL1L at 27°C in *spt16-1* relative to WT after normalization to *act1+*. The TEL1L gene array scheme is shown above the graph. n = 4 biological replicates. Data are presented as the mean ± SEM.

This suggests that heterochromatin nucleation is not affected in the FACT mutant. The gradual reduction of H3K9me2 at subtelomeres (Figure 1B) prompted us to investigate whether FACT plays a role instead in heterochromatin spreading.

Precise analysis of heterochromatin spreading requires the ability to record heterochromatin assembly both at nucleation and distal sites. We applied a recently developed heterochromatin spreading sensor (HSS) assay (Greenstein et al., 2018). In this system, two fluorescent reporters are integrated at different sites to report on heterochromatin nucleation (green) and spreading (orange). An additional red reporter in an unrelated locus is used to filter for cellular noise (Figure 2A). We integrated the HSS reporter at the mating-type locus, since this region has been widely used for studying heterochromatin spreading (Greenstein et al., 2018; Holla et al., 2020; Shipkovenska et al., 2020). We used a genetic background with a

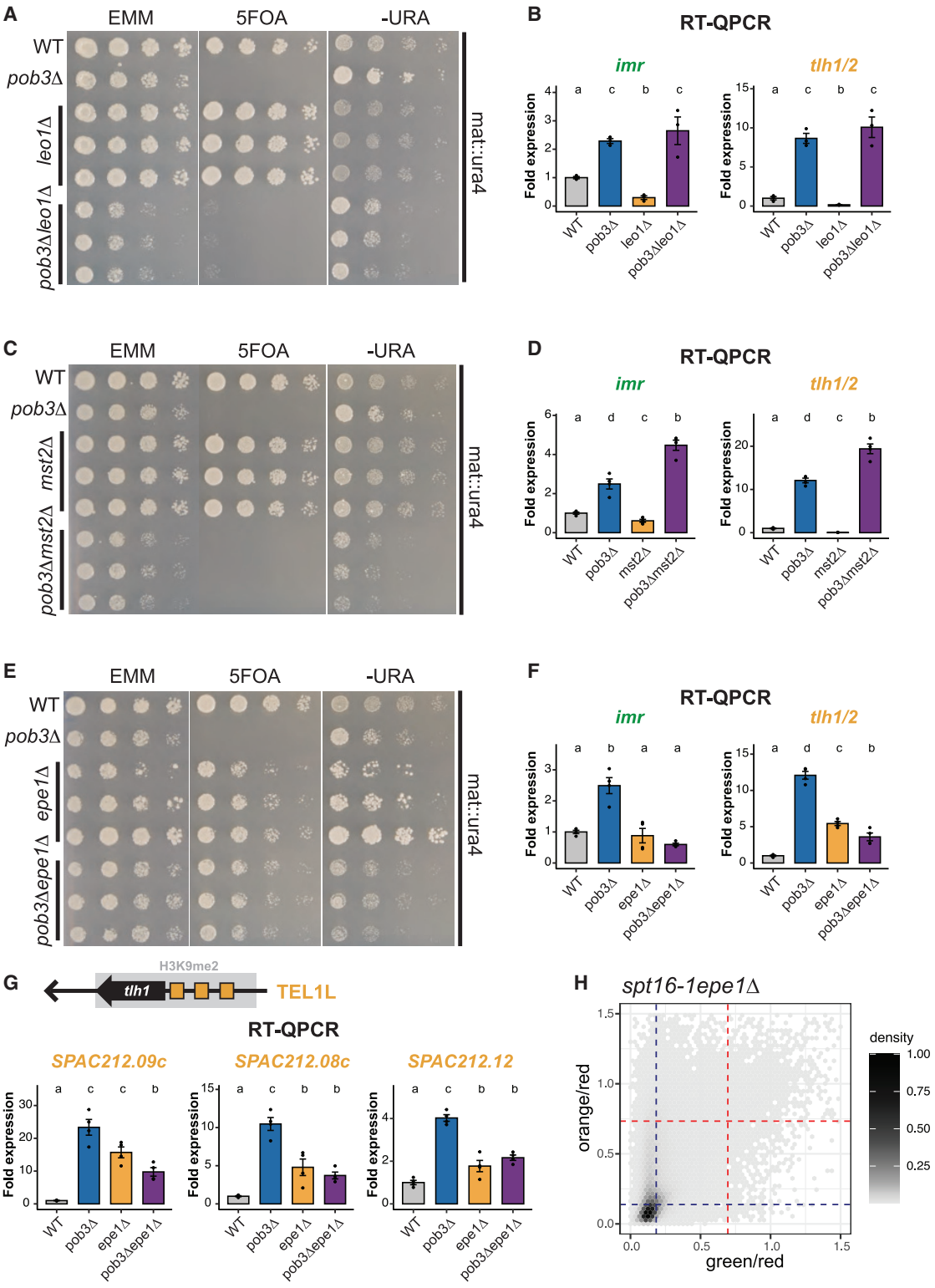

Figure 3. Deletion of *epe1+* suppresses FACT silencing and spreading defects

(A, C, and E) Silencing reporter assay at the *mat* locus. Five-fold serial dilutions of WT, *pob3Δ*, and three independent isolates of the specified single and double mutants were grown on the indicated media.

(legend continued on next page)

mutationally inactivated *REIII* element deficient in recruiting Clr4, HP1, and histone deacetylases via the transcription factors Atf1 and Pcr1 (Figure 2B) (Jia et al., 2004). Hence, heterochromatin nucleation and spreading is driven exclusively from the RNAi-pathway-dependent *cenH* element at the *mat* locus. To quantitatively assess heterochromatin formation, flow cytometry (FC) was done on log-phase cells (Greenstein et al., 2018). FC analysis showed no changes in the cell cycle profiles of mutants deficient in FACT in contrast to the G1/M-arrested *ts cdc25* cells, which served as a control for cell cycle perturbations (Figure S2B). For the control *clr4Δ* strain, in which H3K9me is completely erased, the HSS assay showed derepression of both green and orange reporters compared to the wild-type (WT) strain (Figure 2C). Conversely, in the *pob3Δ* strain, the orange reporter was also fully derepressed in the majority of cells, yet the green reporter remained silenced or mildly derepressed. This result implies that *pob3Δ* cells have a heterochromatin spreading defect (Figure 2C). We next examined Spt16, the other FACT subunit. Since *spt16* deletions are inviable, we used the *ts spt16-1* allele, which contains several point mutations within the N terminus and affects FACT stability at the restrictive temperature (Choi et al., 2012). While *spt16-1* cannot grow at 32°C, it is viable at 27°C but displays a substantial reduction of both Spt16 and Pob3 protein levels at euchromatin and heterochromatin at the nonrestrictive temperature (Figures S2C–S2E). Hence, we concluded that the *spt16-1* mutant is a partial loss-of-FACT-function allele when grown at 27°C, which provides a unique opportunity to study the specific functions of this histone chaperone.

Next, we assessed heterochromatin spreading in the *spt16-1* mutant using the HSS assay. Compared to WT cells grown at 32°C (Figure 2C), the two reporters were fully repressed at 27°C (Figure 2D), which is expected, as heterochromatin spreading is temperature sensitive (Greenstein et al., 2018). In contrast, in *spt16-1* cells, the spreading reporter was partially derepressed, while the nucleation reporter remained largely repressed (Figure 2D), revealing a heterochromatin spreading defect also in this FACT mutant.

Since H3K9me2 was reduced toward the heterochromatic boundaries at subtelomeres in *pob3Δ*, we next investigated potential spreading defects at these loci in *spt16-1*. Even though *spt16-1* does not display silencing defects at pericentromeres at 27°C (Figure S2F), we observed derepression of several subtelomeric genes (Figures 2E and S2G). Remarkably, those derepressed genes are located close to telomere-distal heterochromatin at TEL1L and TEL1R, but not telomere-proximal heterochromatin where nucleation is mediated by shelterin and RNAi. Taken together, our results strongly suggest that FACT has a specific function in heterochromatin spreading at the mating-type and subtelomeric heterochromatin loci.

Epe1 pathway specifically counteracts FACT at heterochromatin

To identify pathways by which FACT contributes to heterochromatin spreading, we investigated potential suppressors of the *pob3Δ* mutant. Several factors counteract heterochromatin spreading, including the histone acetyltransferase Mst2 (Flury et al., 2017; Georgescu et al., 2020; Wang et al., 2015), the transcription elongation complex Paf1C (Kowalik et al., 2015; Sadeghi et al., 2015; Verrier et al., 2015), and the jumonji protein Epe1 that shows homology to histone demethyltransferases and acts as a heterochromatin boundary factor (Ayoub et al., 2003; Braun et al., 2011; Zofall and Grewal, 2006). We generated double mutants of those genes with *pob3Δ* and monitored silencing by growth-based silencing reporter assays and RT-qPCR (Figure 3). Cells lacking *pob3+* showed, as expected, silencing defects for the *ura4+* reporter integrated at the *mat* locus (Figure 3A). Deletions of *leo1+* or *mst2+* did not suppress *pob3Δ* silencing defects at the mating-type locus, pericentromeres, and subtelomeres (Figures 3A–3D). This result is in agreement with the main functions of these factors in maintaining euchromatin by preventing spreading of heterochromatin or the ectopic assembly beyond its natural boundaries. In contrast, deletion of *epe1+* suppressed the *pob3Δ* silencing defects nearly to levels as in the WT cells at all tested heterochromatic regions (Figures 3E and 3F). Moreover, *epe1Δ* reduced the expression of several subtelomeric genes in *pob3Δ*, suggesting that it also counteracts heterochromatin spreading (Figure 3G). To test this more directly, we performed the HSS assay in the double *spt16-1epe1Δ* mutant. Indeed, heterochromatin spreading was completely restored (Figure 3H, compare with Figure 2D). Together, our suppressor analysis revealed that the Epe1 pathway specifically suppresses silencing and spreading defects of FACT mutants, supporting the distinct function of FACT in heterochromatin spreading.

Epe1 is recruited to heterochromatin via Swi6, which binds to H3K9me3 (Zofall and Grewal, 2006). The specific suppression of the FACT spreading defects by *epe1Δ* raised the possibility that Epe1 steady-state levels or abundance at heterochromatin are increased in the FACT mutants. To test this, we examined Epe1 turnover, which is mediated by the Cul4-Ddb1-Cdt2 ubiquitin ligase complex in S phase (Braun et al., 2011). Although degradation of Epe1 still occurs in *pob3Δ* in S phase, we found increased steady-state levels of Epe1 in cycling cells (Figure S3A). This may suggest that Epe1 accumulates at heterochromatin when FACT is impaired. However, ChIP-qPCR of

(B, D, and F) RT-qPCR analysis. Expression of *imr* and *tlh1/2* transcripts in the indicated strains relative to WT after normalization to *act1+*. n = 3 (B) or 4 (D and F) biological replicates. Data are presented as the mean ± SEM. One-way ANOVA was done on log2-transformed values. Different letters denote significant differences with a Tukey post hoc test at $p < 0.05$.

(G) RT-qPCR analysis. Expression of transcripts at TEL1L in *pob3Δ*, *epe1Δ*, and *pob3Δepe1Δ* relative to WT after normalization to *act1+*. n = 4 biological replicates. Data are presented as the mean ± SEM. One-way ANOVA was done on log2-transformed values. Different letters denote significant differences with a Tukey post hoc test at $p < 0.05$.

(H) Two-dimensional-density hexbin plot showing the red-normalized green and orange fluorescence for *spt16-1epe1Δ* MAT_REIIIΔ cells grown at 27°C. Three independent isolates were analyzed and are shown in a combined plot. Labeling as in Figure 2C.

See also Figure S3 and Table S3.

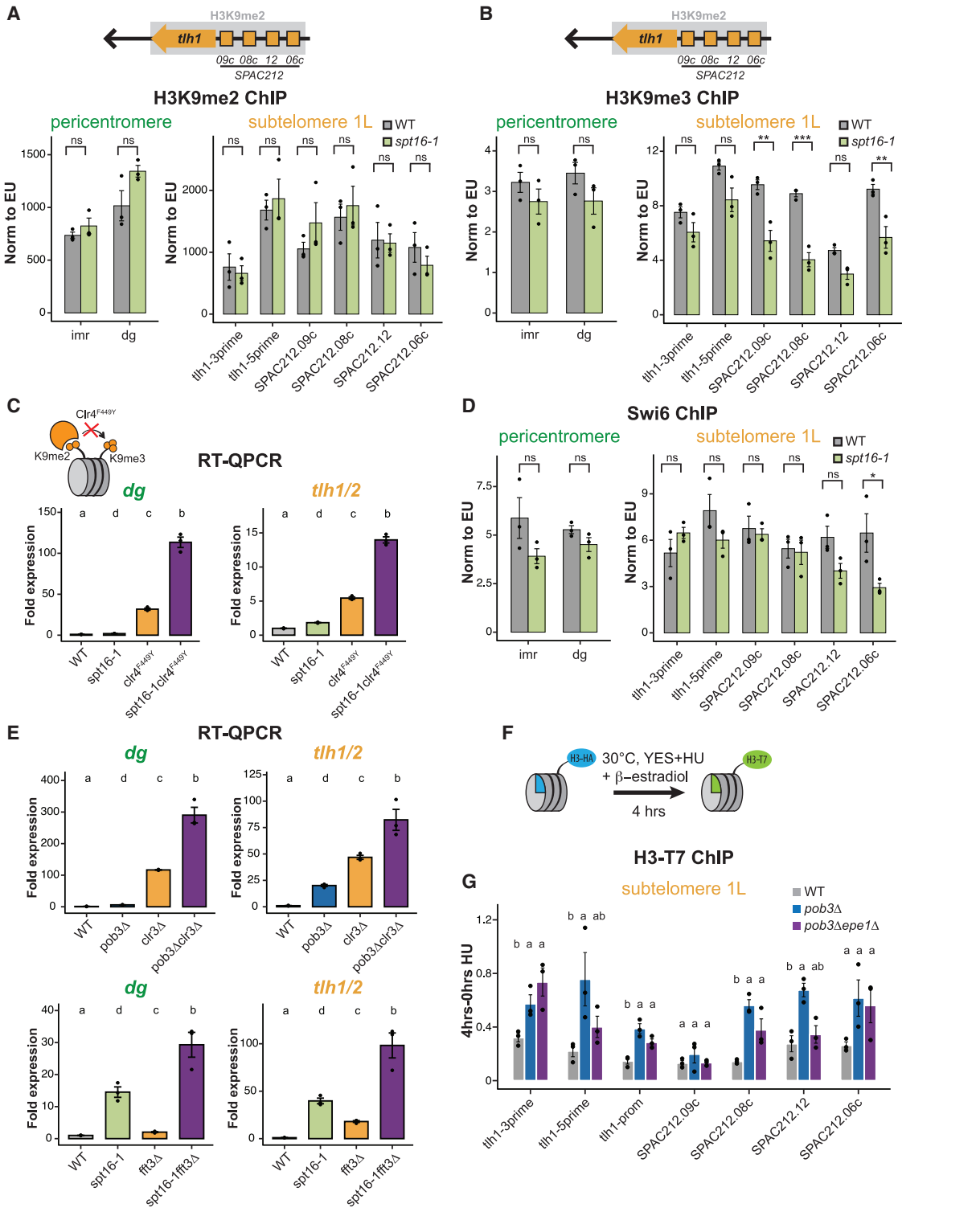

Figure 4. FACT facilitates H3K9me2 to H3Kme3 transition by suppressing histone turnover

(A, B, and D) H3K9me2 (A), H3K9me3 (B), and Swi6 (D) ChIP-qPCR at pericentromeres and TEL1L in WT and *spt16-1*. The TEL1L gene array is shown above the graphs. ChIP was normalized to the average of three euchromatic regions. n = 3 biological replicates. Data are presented as the mean ± SEM. The p values were obtained by linear mixed effect regression (*p < 0.05; **p < 0.01; ***p < 0.001). ns, not significant (p ≥ 0.05).

(legend continued on next page)

Epe1 in *pob3Δ* and *spt16-1* showed no increased signal of Epe1 at pericentromeres or subtelomeres (Figure S3B). Instead, we found decreased levels of Epe1 at subtelomeres in *pob3Δ*, consistent with reduced H3K9me2 at those loci. Based on these findings, we reasoned that the spreading defect in FACT mutants is likely not due to increased Epe1 accumulation at heterochromatin. However, it is possible that heterochromatin alterations in FACT mutants promote transient Epe1 binding that cannot be captured by ChIP assays.

FACT promotes the transition of H3K9me2 to H3K9me3 through histone turnover suppression

Having established a function of FACT in heterochromatin spreading, we sought to elucidate the underlying mechanism and inspected the heterochromatin structure in the *spt16-1* mutant. H3K9me2 and H3K9me3 have distinct heterochromatic functions. H3K9me2 domains are transcriptionally active and sufficient for RNAi-dependent cotranscriptional gene silencing (Jih et al., 2017). Conversely, H3K9me3-marked chromatin is refractory to transcription, directs RNAi-independent gene silencing, and preferentially retains Swi6 (Jih et al., 2017; Schalch et al., 2009; Yamada et al., 2005). Intriguingly, while H3K9me2 levels were unaltered in *spt16-1*, H3K9me3 levels were reduced at several loci at the TEL1L subtelomeric region (i.e., SPAC212.09c, SPAC212.08c, and SPAC212.06c; compare Figure 4B with 4A). This was not seen at pericentromeres, which are mainly cotranscriptionally repressed through RNAi. This was also different from *pob3Δ* cells, which showed a significant decrease of H3K9me2 at subtelomeres (Figure 1B), suggesting that *pob3Δ* displays broader phenotypes, possibly due to pleiotropic and/or indirect effects. Next, we combined the *spt16-1* allele with a clr4^{F449Y} mutant impaired in the transition from H3K9me2 to H3K9me3 (Jih et al., 2017) and observed a synthetic defect in the silencing of *dg* and *tlh1/2* transcripts (Figure 4C). Since efficient heterochromatin spreading requires a self-propagating loop of H3K9 methylation and Swi6 binding, we also monitored Swi6 and found reduced Swi6 binding in *spt16-1* at subtelomeric genes close to the heterochromatin boundary (SPAC212.12, SPAC212.06c; Figure 4D). Together, our results suggest that the H3K9me2/me3 transition is impaired in *spt16-1*, which likely impairs the heterochromatin spreading process.

How can a histone chaperone facilitate the transition of H3K9me2 to H3K9me3? In contrast to mono- and dimethylation, the methylation rate of H3K9me3 by Clr4 is very slow (Al-Sady et al., 2013). The molecular mechanism of this reaction step is not fully understood. Histone turnover rates are critical for establishing methylation states (Chory et al., 2019), and an increased histone turnover was shown in *pob3Δ* for the mating-type locus (Holla et al., 2020). Thus, we hypothesized that increased histone turnover in the absence of FACT impairs H3K9 trimethylation by Clr4. Indeed, both *pob3Δ* and *spt16-1* strains showed synthetic genetic interactions with two factors known to repress histone turnover at heterochromatin, the histone deacetylase Clr3 (Aygün et al., 2013) and the chromatin remodeler Fft3 (Taneja et al., 2017) (Figure 4E). Histone H3 ChIP-seq revealed a small but reproducible reduction of H3 at subtelomeres in *pob3Δ* (Figures S4A–S4C). This subtle histone change may indicate increased nucleosome instability due to elevated histone turnover. To test this further, we used the recombination-induced tag exchange (RITE) approach (Svensson et al., 2015) to monitor incorporation of new H3 histones tagged with a T7 epitope (Figure 4F). Both WT and *pob3Δ* strains displayed similar tag switch recombination rates (76.5% for WT versus 73.4% for *pob3Δ*) and H3-T7 signals were not increased at a control euchromatic gene (Figure S4D). Nonetheless, the *pob3Δ* mutant exhibited increased incorporation of H3-T7 at the TEL1L region (Figure 4G), implying that the H3 turnover rate is increased at subtelomeric heterochromatin.

Since Epe1 was implicated in promoting histone turnover (Aygün et al., 2013), we tested whether *epe1+* deletion suppresses elevated histone turnover in the FACT mutant. Using the RITE approach, we found that histone turnover was partially decreased in the double *pob3Δepe1Δ* mutant compared to *pob3Δ* at various subtelomeric loci (tlh1-5prime and SPAC212.12; Figures 4G and S4D), which correlated with reduced RNAPII levels at this region (Figure S4E). We concluded that suppression of heterochromatin spreading by *epe1Δ* in the FACT mutants is related to the role of Epe1 in promoting histone turnover, likely through heterochromatin transcription (Aygün et al., 2013; Bao et al., 2019; Zofall and Grewal, 2006). Altogether, our data indicate that FACT regulates heterochromatin spreading by promoting the transition of H3K9me2 to H3K9me3 by histone turnover suppression.

DISCUSSION

The involvement of FACT in heterochromatin silencing has been appreciated for a long time; however, the underlying mechanisms have been unclear (Holla et al., 2020; Lejeune et al., 2007). One limiting factor of previous studies was the usage of the *pob3Δ* strain, which due to its strong silencing and pleiotropic effects likely masked specific roles of FACT in heterochromatin formation. Here, by using a partial loss of function, the *spt16-1* ts allele, we were able to show that FACT specifically promotes heterochromatin spreading. First, we show with the HSS assay that the spreading reporter is derepressed, while the nucleation reporter remains largely silenced in both the *pob3Δ* and *spt16-1* mutants. Second, genes distal from nucleation sites at subtelomeric heterochromatin are derepressed in *spt16-1*. Third, H3K9me3 and Swi6 binding, but not H3K9me2,

(C and E) RT-qPCR analysis. Expression of *dg* and *tlh1/2* transcripts in the indicated strains relative to WT after normalization to *act1+*. The *spt16-1*, *fft3Δ*, *spt16-1fft3Δ*, and corresponding WT were shifted to 37°C for 1.5 h. n = 3 biological replicates. Data are presented as the mean ± SEM. One-way ANOVA was done on log2-transformed values. Different letters denote significant differences with a Tukey post hoc test at $p < 0.05$.
(F) Histone turnover assay scheme.
(G) ChIP-qPCR of the new histone (H3-T7) at TEL1L in WT, *pob3Δ*, and *pob3Δepe1Δ*. Input-normalized ChIP signals from the uninduced samples (0 h) were subtracted from the input-normalized signals from the β-estradiol-induced samples (4 h). Error bars represent ± SEM from three independent experiments. One-way ANOVA was done on log2-transformed values. Different letters denote significant differences with a Tukey post hoc test at $p < 0.05$.
See also Figure S4 and Table S3.

is reduced in *spt16-1* at subtelomeric heterochromatin. Fourth, FACT acts synergistically with the Clr4 H3K9me2/me3 transition mutant. Finally, deletion of *epe1+*, which counteracts heterochromatin spreading, suppresses most of the silencing and spreading defects of the FACT mutants. Based on our results, we propose that FACT maintains a low level of histone turnover, which enables a productive H3K9 trimethylation step by Clr4 and heterochromatin spreading.

Our studies are in agreement with the idea that the histone turnover rate is crucial for determination of the genome methylation states (Becker et al., 2016; Chory et al., 2019). Particularly low histone turnover may be important for enzymes with slow kinetic rates, like Clr4 that generates H3K9me3 roughly 10 times slower than H3K9me1 and H3K9me2 (Al-Sady et al., 2013). Similar slow kinetic properties are found for the human K9 and K27 methyltransferases, G9a (Patnaik et al., 2004) and EZH2 (Alabert et al., 2020; Chory et al., 2019), respectively. Thus, low histone turnover emerges as a critical factor for the establishment of repressive chromatin domains.

How is FACT involved in H3K9me3 maintenance and low histone turnover? The efficiency of adjacent nucleosome methylation by Clr4, and thus heterochromatin spreading, likely depends on the retention of the enzyme on the already methylated substrate. FACT could, as at euchromatin, passively maintain methylated histones by preventing heterochromatin "scrambling" (Jeronimo et al., 2019; Svensson et al., 2015). In this scenario, impaired euchromatic and heterochromatic histone reassembly in the FACT mutants would lead to an increased pool of soluble histones, which could be randomly incorporated into the genome, including heterochromatin. This would result in increased histone replacement and reduced H3K9me, which in turn could open a window of opportunity for the transcription machinery to bind to heterochromatin. Alternatively, transcription itself could contribute to the increased histone turnover in the FACT mutants. In that case, FACT would maintain low histone turnover by blocking access of RNAPII to heterochromatic regions. This notion is supported by results from our RNAPII ChIP-seq analysis and identification of suppressors linked to transcription elongation or termination (*paf1*, *res2*) or to promotion of heterochromatin transcription (*epe1*). This suggests that FACT protects heterochromatin from illegitimate transcription and likely transcription-induced histone turnover. A recent study revealed that FACT is recruited to heterochromatin via an interaction with the chromoshadow domain of Swi6 (Takahata et al., 2021). It is thus tempting to speculate that this interaction keeps FACT in the vicinity of heterochromatin and together with other silencing factors creates a physical barrier for RNAPII and histone replacement, which would promote the H3K9me3 state. In this scenario, FACT would have a more "active" role in maintaining low heterochromatic histone turnover. Our results cannot unambiguously distinguish between those two models and further studies are needed to clarify this.

Histone turnover is linked to heterochromatin inheritance and heritable changes in gene expression patterns (Aygün et al., 2013; Greenstein et al., 2018; Holla et al., 2020; Shan et al., 2020; Taneja et al., 2017). Our results support the findings that histone chaperones that guide heterochromatic histone turnover may be involved in controlling cell fate (Brumbaugh et al., 2019; Cheloufi et al., 2015; Kolundzic et al., 2018). Future studies should address whether FACT function in heterochromatin spreading is conserved in metazoan development and cell fate maintenance.

Limitations of study

Our analysis revealed important differences between the two FACT mutants. While H3K9me2 levels are gradually reduced from the subtelomeric nucleation sites in *pob3Δ*, H3K9me2 is not changed in *spt16-1*. In contrast to *pob3Δ*, which has strong silencing defects throughout heterochromatin, *spt16-1* shows derepression of genes primarily at heterochromatin boundaries that are distal from nucleation sites, in agreement with its defects in heterochromatin spreading. One limitation of the study is that due to strong silencing defects of the *pob3Δ* allele, we cannot exclude that some of the observed phenotypes are indirect. However, the specific spreading defect seen in the partial loss-of-function *spt16-1* mutant suggests that heterochromatin spreading regulation is indeed the main function of FACT at heterochromatin. Thus, our results highlight the importance of hypomorphic mutants for studying abundant and pleiotropic protein complexes.

STAR★METHODS

Detailed methods are provided in the online version of this paper and include the following:

- KEY RESOURCES TABLE
- RESOURCE AVAILABILITY
  - Lead contact
  - Materials availability
  - Data and code availability
- EXPERIMENTAL MODEL AND SUBJECT DETAILS
- METHOD DETAILS
  - RNA extraction and cDNA synthesis
  - Gene expression analysis
  - ChIP-seq and ChIP-qPCR
  - ChIP-seq analysis
  - Histone turnover assay
  - Protein extract preparation
  - Western blot
  - HSS assay
  - Cell cycle analysis
- QUANTIFICATION AND STATISTICAL ANALYSIS

SUPPLEMENTAL INFORMATION

Supplemental information can be found online at https://doi.org/10.1016/j.celrep.2021.109944.

ACKNOWLEDGMENTS

We thank LAFUGA, Stefan Krebs, and Helmut Blum for sequencing. We thank Julia Schluckebier for assistance in strain generation. This research was supported by the European Commission (Marie-Curie Individual Fellowship H2020-MSCA-IF-2014 contract 657244 to M.M. and Network of Excellence EpiGeneSys HEALTH-2010-257082 to A.G.L. and S.B.), the Friedrich-Baur-Stiftung (to M.M. and S.B.), the DFG (projects 213249687-SFB 1064 and 325871075-SFB 1309 to A.G.L. and project 453441129 to M.M.), the National Institutes of Health (grant DP2GM123484 to B.A.-S.), the National Science

Foundation (grant 2113319 to B.A.-S.), and the University of California, San Francisco Program for Breakthrough Biomedical Research (to B.A.-S.).

AUTHOR CONTRIBUTIONS

Conceptualization, M.M., S.B., B.A.-S., and A.G.L.; investigation, M.M., R.A.G., K.C.F.O., H.N., and B.A.-S.; formal analysis, M.M., T.S., and R.A.G.; visualization, M.M., T.S., R.A.G., and B.A.-S.; resources, S.B., B.A.-S., and A.G.L.; writing – original draft, M.M.; writing – review & editing, M.M., S.B., B.A.-S., and A.G.L.; funding acquisition, M.M., S.B., B.A.-S., and A.G.L.

DECLARATION OF INTERESTS

A.G.L. is a founder, CSO, shareholder, and managing director of Eisbach Bio GmbH, a biotechnology company developing cancer medicines. All other authors declare no competing interests.

Received: July 19, 2021
Revised: September 14, 2021
Accepted: October 13, 2021
Published: November 2, 2021

REFERENCES

Al-Sady, B., Greenstein, R.A., El-Samad, H.J., Braun, S., and Madhani, H.D. (2016). Sensitive and Quantitative Three-Color Protein Imaging in Fission Yeast Using Spectrally Diverse, Recoded Fluorescent Proteins with Experimentally-Characterized In Vivo Maturation Kinetics. PLoS ONE *11*, e0159292.

Al-Sady, B., Madhani, H.D., and Narlikar, G.J. (2013). Division of labor between the chromodomains of HP1 and Suv39 methylase enables coordination of heterochromatin spread. Mol. Cell *51*, 80–91.

Alabert, C., Loos, C., Voelker-Albert, M., Graziano, S., Forné, I., Reveron-Gomez, N., Schuh, L., Hasenauer, J., Marr, C., Imhof, A., and Groth, A. (2020). Domain Model Explains Propagation Dynamics and Stability of Histone H3K27 and H3K36 Methylation Landscapes. Cell Rep. *30*, 1223–1234.e8.

Allshire, R.C., and Ekwall, K. (2015). Epigenetic Regulation of Chromatin States in Schizosaccharomyces pombe. Cold Spring Harb. Perspect. Biol. *7*, a018770.

Aygün, O., Mehta, S., and Grewal, S.I. (2013). HDAC-mediated suppression of histone turnover promotes epigenetic stability of heterochromatin. Nat. Struct. Mol. Biol. *20*, 547–554.

Ayoub, N., Noma, K., Isaac, S., Kahan, T., Grewal, S.I., and Cohen, A. (2003). A novel jmjC domain protein modulates heterochromatization in fission yeast. Mol. Cell. Biol. *23*, 4356–4370.

Bao, K., Shan, C.M., Moresco, J., Yates, J., 3rd, and Jia, S. (2019). Anti-silencing factor Epe1 associates with SAGA to regulate transcription within heterochromatin. Genes Dev. *33*, 116–126.

Barrales, R.R., Forn, M., Georgescu, P.R., Sarkadi, Z., and Braun, S. (2016). Control of heterochromatin localization and silencing by the nuclear membrane protein Lem2. Genes Dev. *30*, 133–148.

Becker, J.S., Nicetto, D., and Zaret, K.S. (2016). H3K9me3-Dependent Heterochromatin: Barrier to Cell Fate Changes. Trends Genet. *32*, 29–41.

Braun, S., Garcia, J.F., Rowley, M., Rougemaille, M., Shankar, S., and Madhani, H.D. (2011). The Cul4-Ddb1(Cdt)^2 ubiquitin ligase inhibits invasion of a boundary-associated antisilencing factor into heterochromatin. Cell *144*, 41–54.

Brumbaugh, J., Di Stefano, B., and Hochedlinger, K. (2019). Reprogramming: identifying the mechanisms that safeguard cell identity. Development *146*, dev182170.

Cheloufi, S., Elling, U., Hopfgartner, B., Jung, Y.L., Murn, J., Ninova, M., Hubmann, M., Badeaux, A.I., Euong Ang, C., Tenen, D., et al. (2015). The histone chaperone CAF-1 safeguards somatic cell identity. Nature *528*, 218–224.

Chen, E.S., Zhang, K., Nicolas, E., Cam, H.P., Zofall, M., and Grewal, S.I. (2008). Cell cycle control of centromeric repeat transcription and heterochromatin assembly. Nature *451*, 734–737.

Choi, E.S., Strålfors, A., Catania, S., Castillo, A.G., Svensson, J.P., Pidoux, A.L., Ekwall, K., and Allshire, R.C. (2012). Factors that promote H3 chromatin integrity during transcription prevent promiscuous deposition of CENP-A(Cnp1) in fission yeast. PLoS Genet. *8*, e1002985.

Chory, E.J., Calarco, J.P., Hathaway, N.A., Bell, O., Neel, D.S., and Crabtree, G.R. (2019). Nucleosome Turnover Regulates Histone Methylation Patterns over the Genome. Mol. Cell *73*, 61–72.e3.

Duina, A.A., Rufiange, A., Bracey, J., Hall, J., Nourani, A., and Winston, F. (2007). Evidence that the localization of the elongation factor Spt16 across transcribed genes is dependent upon histone H3 integrity in Saccharomyces cerevisiae. Genetics *177*, 101–112.

Ekwall, K., Javerzat, J.P., Lorentz, A., Schmidt, H., Cranston, G., and Allshire, R. (1995). The chromodomain protein Swi6: a key component at fission yeast centromeres. Science *269*, 1429–1431.

Flury, V., Georgescu, P.R., Iesmantavicius, V., Shimada, Y., Kuzdere, T., Braun, S., and Bühler, M. (2017). The Histone Acetyltransferase Mst2 Protects Active Chromatin from Epigenetic Silencing by Acetylating the Ubiquitin Ligase Brl1. Mol. Cell *67*, 294–307.e9.

Formosa, T., and Winston, F. (2020). The role of FACT in managing chromatin: disruption, assembly, or repair? Nucleic Acids Res. *48*, 11929–11941.

Garcia-Luis, J., Lazar-Stefanita, L., Gutierrez-Escribano, P., Thierry, A., Cournac, A., García, A., González, S., Sánchez, M., Jarmuz, A., Montoya, A., et al. (2019). FACT mediates cohesin function on chromatin. Nat. Struct. Mol. Biol. *26*, 970–979.

Georgescu, P.R., Capella, M., Fischer-Burkart, S., and Braun, S. (2020). The euchromatic histone mark H3K36me3 preserves heterochromatin through sequestration of an acetyltransferase complex in fission yeast. Microb. Cell *7*, 80–92.

Goto, D.B., and Nakayama, J. (2012). RNA and epigenetic silencing: insight from fission yeast. Dev. Growth Differ. *54*, 129–141.

Greenstein, R.A., Barrales, R.R., Sanchez, N.A., Bisanz, J.E., Braun, S., and Al-Sady, B. (2020). Set1/COMPASS repels heterochromatin invasion at euchromatic sites by disrupting Suv39/Clr4 activity and nucleosome stability. Genes Dev. *34*, 99–117.

Greenstein, R.A., Jones, S.K., Spivey, E.C., Rybarski, J.R., Finkelstein, I.J., and Al-Sady, B. (2018). Noncoding RNA-nucleated heterochromatin spreading is intrinsically labile and requires accessory elements for epigenetic stability. eLife *7*, e32948.

Heinz, S., Benner, C., Spann, N., Bertolino, E., Lin, Y.C., Laslo, P., Cheng, J.X., Murre, C., Singh, H., and Glass, C.K. (2010). Simple combinations of lineage-determining transcription factors prime cis-regulatory elements required for macrophage and B cell identities. Mol. Cell *38*, 576–589.

Herrera-Moyano, E., Mergui, X., García-Rubio, M.L., Barroso, S., and Aguilera, A. (2014). The yeast and human FACT chromatin-reorganizing complexes solve R-loop-mediated transcription-replication conflicts. Genes Dev. *28*, 735–748.

Holla, S., Dhakshnamoorthy, J., Folco, H.D., Balachandran, V., Xiao, H., Sun, L.L., Wheeler, D., Zofall, M., and Grewal, S.I.S. (2020). Positioning Heterochromatin at the Nuclear Periphery Suppresses Histone Turnover to Promote Epigenetic Inheritance. Cell *180*, 150–164.e15.

Janssen, A., Colmenares, S.U., and Karpen, G.H. (2018). Heterochromatin: Guardian of the Genome. Annu. Rev. Cell Dev. Biol. *34*, 265–288.

Jeronimo, C., Poitras, C., and Robert, F. (2019). Histone Recycling by FACT and Spt6 during Transcription Prevents the Scrambling of Histone Modifications. Cell Rep. *28*, 1206–1218.e8.

Jia, S., Yamada, T., and Grewal, S.I. (2004). Heterochromatin regulates cell type-specific long-range chromatin interactions essential for directed recombination. Cell *119*, 469–480.

Jih, G., Iglesias, N., Currie, M.A., Bhanu, N.V., Paulo, J.A., Gygi, S.P., Garcia, B.A., and Moazed, D. (2017). Unique roles for histone H3K9me states in RNAi and heritable silencing of transcription. Nature *547*, 463–467.

Knop, M., Siegers, K., Pereira, G., Zachariae, W., Winsor, B., Nasmyth, K., and Schiebel, E. (1999). Epitope tagging of yeast genes using a PCR-based strategy: more tags and improved practical routines. Yeast *15* (*10B*), 963–972.

Knutsen, J.H., Rein, I.D., Rothe, C., Stokke, T., Grallert, B., and Boye, E. (2011). Cell-cycle analysis of fission yeast cells by flow cytometry. PLoS ONE *6*, e17175.

Kolundzic, E., Ofenbauer, A., Bulut, S.I., Uyar, B., Baytek, G., Sommermeier, A., Seelk, S., He, M., Hirsekorn, A., Vucicevic, D., et al. (2018). FACT Sets a Barrier for Cell Fate Reprogramming in Caenorhabditis elegans and Human Cells. Dev. Cell *46*, 611–626.e12.

Kowalik, K.M., Shimada, Y., Flury, V., Stadler, M.B., Batki, J., and Bühler, M. (2015). The Paf1 complex represses small-RNA-mediated epigenetic gene silencing. Nature *520*, 248–252.

Langmead, B., and Salzberg, S.L. (2012). Fast gapped-read alignment with Bowtie 2. Nat. Methods *9*, 357–359.

Lawrence, M., Gentleman, R., and Carey, V. (2009). rtracklayer: an R package for interfacing with genome browsers. Bioinformatics *25*, 1841–1842.

Lawrence, M., Huber, W., Pagès, H., Aboyoun, P., Carlson, M., Gentleman, R., Morgan, M.T., and Carey, V.J. (2013). Software for computing and annotating genomic ranges. PLoS Comput. Biol. *9*, e1003118.

Lee, J., Choi, E.S., Seo, H.D., Kang, K., Gilmore, J.M., Florens, L., Washburn, M.P., Choe, J., Workman, J.L., and Lee, D. (2017). Chromatin remodeller $Fun30^{Fft3}$ induces nucleosome disassembly to facilitate RNA polymerase II elongation. Nat. Commun. *8*, 14527.

Lejeune, E., Bortfeld, M., White, S.A., Pidoux, A.L., Ekwall, K., Allshire, R.C., and Ladurner, A.G. (2007). The chromatin-remodeling factor FACT contributes to centromeric heterochromatin independently of RNAi. Curr. Biol. *17*, 1219–1224.

Liu, Y., Zhou, K., Zhang, N., Wei, H., Tan, Y.Z., Zhang, Z., Carragher, B., Potter, C.S., D'Arcy, S., and Luger, K. (2020). FACT caught in the act of manipulating the nucleosome. Nature *577*, 426–431.

Lun, A.T., and Smyth, G.K. (2016). csaw: a Bioconductor package for differential binding analysis of ChIP-seq data using sliding windows. Nucleic Acids Res. *44*, e45.

Martienssen, R., and Moazed, D. (2015). RNAi and heterochromatin assembly. Cold Spring Harb. Perspect. Biol. *7*, a019323.

Mizuguchi, T., Barrowman, J., and Grewal, S.I. (2015). Chromosome domain architecture and dynamic organization of the fission yeast genome. FEBS Lett. *589* (*20 Pt A*), 2975–2986.

Murawska, M., Schauer, T., Matsuda, A., Wilson, M.D., Pysik, T., Wojcik, F., Muir, T.W., Hiraoka, Y., Straub, T., and Ladurner, A.G. (2020). The Chaperone FACT and Histone H2B Ubiquitination Maintain S. pombe Genome Architecture through Genic and Subtelomeric Functions. Mol. Cell *77*, 501–513.e7.

Orphanides, G., LeRoy, G., Chang, C.H., Luse, D.S., and Reinberg, D. (1998). FACT, a factor that facilitates transcript elongation through nucleosomes. Cell *92*, 105–116.

Patnaik, D., Chin, H.G., Estève, P.O., Benner, J., Jacobsen, S.E., and Pradhan, S. (2004). Substrate specificity and kinetic mechanism of mammalian G9a histone H3 methyltransferase. J. Biol. Chem. *279*, 53248–53258.

Penagos-Puig, A., and Furlan-Magaril, M. (2020). Heterochromatin as an Important Driver of Genome Organization. Front. Cell Dev. Biol. *8*, 579137.

Reyes-Turcu, F.E., and Grewal, S.I. (2012). Different means, same end-heterochromatin formation by RNAi and RNAi-independent RNA processing factors in fission yeast. Curr. Opin. Genet. Dev. *22*, 156–163.

Robinson, M.D., McCarthy, D.J., and Smyth, G.K. (2010). edgeR: a Bioconductor package for differential expression analysis of digital gene expression data. Bioinformatics *26*, 139–140.

Sadeghi, L., Prasad, P., Ekwall, K., Cohen, A., and Svensson, J.P. (2015). The Paf1 complex factors Leo1 and Paf1 promote local histone turnover to modulate chromatin states in fission yeast. EMBO Rep. *16*, 1673–1687.

Sadeghi, L., Siggens, L., Svensson, J.P., and Ekwall, K. (2014). Centromeric histone H2B monoubiquitination promotes noncoding transcription and chromatin integrity. Nat. Struct. Mol. Biol. *21*, 236–243.

Schalch, T., Job, G., Noffsinger, V.J., Shanker, S., Kuscu, C., Joshua-Tor, L., and Partridge, J.F. (2009). High-affinity binding of Chp1 chromodomain to K9 methylated histone H3 is required to establish centromeric heterochromatin. Mol. Cell *34*, 36–46.

Shan, C.M., Bao, K., Diedrich, J., Chen, X., Lu, C., Yates, J.R., 3rd, and Jia, S. (2020). The INO80 Complex Regulates Epigenetic Inheritance of Heterochromatin. Cell Rep. *33*, 108561.

Shipkovenska, G., Durango, A., Kalocsay, M., Gygi, S.P., and Moazed, D. (2020). A conserved RNA degradation complex required for spreading and epigenetic inheritance of heterochromatin. eLife *9*, e54341.

Svensson, J.P., Shukla, M., Menendez-Benito, V., Norman-Axelsson, U., Audergon, P., Sinha, I., Tanny, J.C., Allshire, R.C., and Ekwall, K. (2015). A nucleosome turnover map reveals that the stability of histone H4 Lys20 methylation depends on histone recycling in transcribed chromatin. Genome Res. *25*, 872–883.

Takahata, S., Chida, S., Ohnuma, A., Ando, M., Asanuma, T., and Murakami, Y. (2021). Two secured FACT recruitment mechanisms are essential for heterochromatin maintenance. Cell Rep. *36*, 109540.

Taneja, N., Zofall, M., Balachandran, V., Thillainadesan, G., Sugiyama, T., Wheeler, D., Zhou, M., and Grewal, S.I. (2017). SNF2 Family Protein Fft3 Suppresses Nucleosome Turnover to Promote Epigenetic Inheritance and Proper Replication. Mol. Cell *66*, 50–62.e6.

Torres-Garcia, S., Di Pompeo, L., Eivers, L., Gaborieau, B., White, S.A., Pidoux, A.L., Kanigowska, P., Yaseen, I., Cai, Y., and Allshire, R.C. (2020). *SpEDIT*: A fast and efficient CRISPR/Cas9 method for fission yeast. Wellcome Open Res. *5*, 274.

van Emden, T.S., Forn, M., Forné, I., Sarkadi, Z., Capella, M., Martín Caballero, L., Fischer-Burkart, S., Brönner, C., Simonetta, M., Toczyski, D., et al. (2019). Shelterin and subtelomeric DNA sequences control nucleosome maintenance and genome stability. EMBO Rep. *20*, e47181.

Verrier, L., Taglini, F., Barrales, R.R., Webb, S., Urano, T., Braun, S., and Bayne, E.H. (2015). Global regulation of heterochromatin spreading by Leo1. Open Biol. *5*, 150045.

Wang, J., Cohen, A.L., Letian, A., Tadeo, X., Moresco, J.J., Liu, J., Yates, J.R., 3rd, Qiao, F., and Jia, S. (2016). The proper connection between shelterin components is required for telomeric heterochromatin assembly. Genes Dev. *30*, 827–839.

Wang, J., Reddy, B.D., and Jia, S. (2015). Rapid epigenetic adaptation to uncontrolled heterochromatin spreading. eLife *4*, e06179.

Wang, X., and Moazed, D. (2017). DNA sequence-dependent epigenetic inheritance of gene silencing and histone H3K9 methylation. Science *356*, 88–91.

Yamada, T., Fischle, W., Sugiyama, T., Allis, C.D., and Grewal, S.I. (2005). The nucleation and maintenance of heterochromatin by a histone deacetylase in fission yeast. Mol. Cell *20*, 173–185.

Zhang, K., Mosch, K., Fischle, W., and Grewal, S.I. (2008). Roles of the Clr4 methyltransferase complex in nucleation, spreading and maintenance of heterochromatin. Nat. Struct. Mol. Biol. *15*, 381–388.

Zofall, M., and Grewal, S.I. (2006). Swi6/HP1 recruits a JmjC domain protein to facilitate transcription of heterochromatic repeats. Mol. Cell *22*, 681–692.

STAR★METHODS

KEY RESOURCES TABLE

REAGENT or RESOURCE	SOURCE	IDENTIFIER
Antibodies		
anti-H3K9me2	Abcam	Ab1220; RRID:AB_449854
anti-H3K9me3	Merck	Cat#07-442; RRID:AB_310620
anti-Swi6	Abcam	Ab188276
anti-H3 clone 1B1-B2	Active Motif	Cat#61475; RRID:AB_2687473
anti-H2Bub clone 56	Active Motif	Cat#39623; RRID:AB_2793279
anti-Pol IISer2 clone 3E10	Dirk Eick Lab	N/A
anti-Pob3	Murawska et al. (2020)	N/A
anti-Spt16	Murawska et al. (2020)	N/A
anti-PCNA (PC10)	Santa Cruz	sc-56; RRID:AB_628110
anti-HA	Sigma	H6908; RRID:AB_260070
anti-Flag	Sigma	F7425; RRID:AB_439687
anti-T7	Merck	69522–3; RRID:AB_11211744
anti-rabbit IgG HRP conjugate	BioRad	Cat#1706515; RRID:AB_2617112
anti-mouse IgG HRP conjugate	BioRad	Cat#1706516; RRID:AB_11125547
anti-rabbit IgG, highly cross-adsorbed, CF™ 680	Sigma	SAB4600200
anti-mouse IgG, highly cross-adsorbed CF™ 680	Sigma	SAB4600199; RRID:AB_2819153
Bacterial and virus strains		
Escherichia coli XL1-blue	Ladurner Lab	N/A
Chemicals, peptides, and recombinant proteins		
TRIzol Reagent	ThermoFisher	Cat#15596026
Superscript III Reverse Transcriptase	Invitrogen	18080085
PowerUp SYBR® Green Master Mix	ThermoFisher	A25742
PowerTrack SYBR® Green Master Mix	ThermoFisher	A46109
NEBNext® Poly(A) mRNA Magnetic Isolation Module	New England Biolabs	E7490S
Zymolyase 100T	Nacalai Tesque, Japan	07665-55
Proteinase K	Sigma	Cat#3115801001
Agencourt AMPure XP beads	BeckmanCoulter	A63880
Dynabeads Protein G	ThermoFisher	Cat#10009D
Phiusion HF DNA polymerase	New England Biolabs	M0530S
Zymo Research ChIP DNA Clean & Concentrator	Zymo Research	Cat#D2505
Immobilon Western HRP Substrate	Millipore	WBKLS0500
cOmplete™ Protease Inhibitor Cocktail	Roche	Cat#11697498001
Benzonase® Nuclease	Sigma	Cat#E1014
Hydroxyurea	Sigma	Cal#H8627
β-estradiol	Sigma	Cal#E8875
Hygromycin B	ThermoFisher	Cat#10687010
Immobilon-FL PVDF	Merck	Cat#IPFL00005
Roti®PVDF	Roth	Cat#T830.1

(*Continued on next page*)

Continued

REAGENT or RESOURCE	SOURCE	IDENTIFIER
Critical commercial assays		
TURBO DNA-*free* Kit	ThermoFisher	AM1907
NEBNext® Ultra II DNA Library Prep Kit for Illumina®	New England Biolabs	E7645S
NEBNext® Multiplex Oligos for Illumina® (Index Primers Set 2)	New England Biolabs	E7500S
Qubit dsDNA HS Assay Kit	ThermoFisher	Q32851
High Sensitivity DNA Assay	Agilent	Cat#5067-4627
NEB Golden Gate Assembly Kit (BsaI-HFv2)	New England Biolabs	Cat#E1601S
Deposited Data		
H3K9me2 ChIP-seq in *pob3Δ*	This study	GEO: GSE174641
Raw western blot images	This study	N/A
Code for the data analysis	This study	https://doi.org/10.5281/zenodo.5564796
Experimental models: Organisms/strains		
S. pombe	This study	Table S1
Oligonucleotides		
RT-QPCR, ChIP-QPCR, cloning	This study	Table S2
Recombinant DNA		
pLSB	Torres-Garcia et al. (2020)	N/A
Software and algorithms		
bowtie2 (version 2.2.9)	Langmead and Salzberg (2012)	http://bowtie-bio.sourceforge.net/bowtie2/index.shtml
csaw R/Bioconductor (version 1.18.0)	Lun and Smyth (2016)	https://bioconductor.org/packages/release/bioc/html/csaw.html
edgeR package (version 3.26.8)	Robinson et al. (2010)	https://bioconductor.org/packages/release/bioc/html/edgeR.html
GenomicRanges package (version 1.38.0)	Lawrence et al. (2013)	https://bioconductor.org/packages/release/bioc/html/GenomicRanges.html
rtracklayer package (version 1.44.4)	Lawrence et al. (2009)	https://www.bioconductor.org/packages/release/bioc/html/rtracklayer.html
zoo package (version 1.8.9)	Cran.R	https://cran.r-project.org/
Homer	Heinz et al. (2010)	http://homer.ucsd.edu/homer/
R (version 4.0.5)	Cran.R	https://cran.r-project.org/
RStudio (version 1.4.1103)	RStudio	https://www.rstudio.com/
flowCore_2.2.0	Bioconductor	https://bioconductor.org/packages/release/bioc/html/flowCore.html
ggplot2	Cran.R	https://ggplot2.tidyverse.org/
lme4 (version 1.1-27)	Cran.R	https://cran.r-project.org/web/packages/lme4/index.html
lmerTest (version 3.1-3)	Cran.R	https://cran.r-project.org/web/packages/lmerTest/index.html
tidyverse_1.3.1	Cran.R	https://tidyverse.tidyverse.org/
hexbin_1.28.2	GitHub	https://cran.r-project.org/web/packages/hexbin/index.html
gridExtra_2.3	Cran.R	https://cran.r-project.org/web/packages/gridExtra/index.html
CRISPR4P	Torres-Garcia et al. (2020)	http://bahlerweb.cs.ucl.ac.uk/cgi-bin/crispr4p/webapp.py

(*Continued on next page*)

Continued

REAGENT or RESOURCE	SOURCE	IDENTIFIER
GraphPad Prism	GraphPad Software Inc.	https://www.graphpad.com/scientific-software/prism/
QuantStudio™ Design and Analysis Software	ThermoFisher	https://www.thermofisher.com/us/en/home/technical-resources/software-downloads/ab-quantstudio-3-and-5-real-time-pcr-system.html
Image Studio™ Lite	LI-COR Biosciences	https://www.licor.com/bio/image-studio-lite/

RESOURCE AVAILABILITY

Lead contact

Further information and requests for resources and reagents should be directed to and will be fulfilled by the Lead Contact, Sigurd Braun (sigurd.braun@gen.bio.uni-giessen.de) or the Corresponding Contact, Magdalena Murawska (magdalena.murawska@bmc.med.lmu.de).

Materials availability

Yeast strains generated in this study are available upon request.

Data and code availability

- H3K9me2 ChIP-seq data in wild-type and *pob3Δ* strains have been deposited at GEO and are publicly available as of the date of publication. Accession numbers are listed in the key resources table.
- All original code has been deposited at Zenodo and is publicly available as of the date of publication. DOIs are listed in the key resources table.
- Any additional information required to reanalyze the data reported in this paper is available from the lead contact upon request.

EXPERIMENTAL MODEL AND SUBJECT DETAILS

S. pombe strains used in this study are listed in Table S1. Strains were generated with standard procedures using yeast transformation and validated by colony PCR. Point mutants were generated using a CRISPR/Cas9 system according to the published method (Torres-Garcia et al., 2020). All CRISPR/Cas9 generated strains were sequenced to confirm the presence of the mutation. Strains used for RITE assay were generated by crossing out the cdc25-22 allele using random spore analysis. Strains were grown in rich media (YES) at 32°C, 30°C or at 27°C as indicated. For temperature sensitive alleles, strains were grown at 26°C overnight and then they were shifted to 36°C for 1.5 hours. 5-FOA medium contained 1 g/L 5′-fluoroorotic acid.

METHOD DETAILS

RNA extraction and cDNA synthesis

RNA extraction and gene expression analysis were done as described in (Barrales et al., 2016; Murawska et al., 2020). Briefly, 50 mL of yeast culture at OD600 0.5-0.8 was spun down at RT and the pellet was frozen in liquid nitrogen. Cells were thawed on ice and resuspended in 1 mL of TRIzol. 250 μL of zirconia beads were added and cells were broken with Precyllis 24 (Peqlab) for 3x30 s with 5 min rest on ice. The extract was spun down at 13500 rpm at 4°C for 10 min. The cleared lysate was extracted twice with chloroform and spun at 13500 rpm at 4°C for 10 min. The aqueous phase was taken and RNA was precipitated with isopropanol. The pellet was washed twice with 75% EtOH, air-dried and resuspended in 50 μL of RNase free dH20. The RNA concentration and purity were determined by Nano-drop. For RT-QPCR 20 mg of RNA was treated with 1 μL of TURBO DNase I (Ambion) for 1 hr at 37°C. The reaction was inactivated by adding 6 μL of DNase inactivation reagent followed by the manufacturer instructions. For cDNA synthesis 5 μg of total DNase-treated RNA was reverse transcribed with 1 μL of oligo-(dT)20 primers (50 μM) and 0.25 μL of SuperscriptIII (Invitrogen) according to the manufacturer instructions.

Gene expression analysis

cDNAs were quantified by qPCR using Fast SYBR Green Master mix (Life Technologies) and a 7500 Fast real-time PCR system (Applied Biosystems). cDNA was analyzed by qPCR using gene specific primers (Table S2). The quantification was based on a standard curve method obtained with QuantStudioTM Design and Analysis Software. Sheared *S. pombe* genomic DNA was used as a

standard. For gene expression the samples were normalized to *act1* gene. The normalized datasets were shown as relative to the mean value of the WT strain which was set to 1, errors bars were calculated as SEM and displayed accordingly.

ChIP-seq and ChIP-qPCR

ChIP-QPCR and ChIP-seq were performed as described previously (Murawska et al., 2020). Briefly, 100 mL yeast cultures were grown to mid-log phase to OD600 = 0.6. The cultures were cooled down at RT for 10 min and fixed with 1% FA for 20 min at RT on the shaker. Cross-linking was stopped with 150 mM Glycine for 10 min at RT. Cells were washed 2x with 30 mL ice-cold dH2O, the pellet was frozen in liquid nitrogen and kept at −80°C until further processing. Pellets were resuspended in 1 mL FA(1) buffer (50 mM HEPES-KOH, pH 7.5, 150 mM NaCl, 1 mM EDTA, 1% Triton X-100 (v/v), 0,1% NaDeoxycholate (w/v), 0,1% SDS (w/v), supplemented with Roche protease inhibitors. Cells were broken in a bead beater (Precellys): 9x30s (for ChIP-seq or 6x30s for ChIP-QPCR). After centrifugation, the supernatant and the pellet were sonicated for 15 min at 4°C. Chromatin extracts were spun down for 10 min at 14000 rpm at 4°C. Different amount of chromatin was used for different antibodies: 100 μl chromatin (for H3-T7, Spt16, Pob3 ChIP) or 500 μl chromatin (for Pol II-Ser2, H3K9me2, H3K9me3, H2Bub, Swi6, Clr4-HA, Epe1-Flag ChIP). The antibodies used for ChIP are listed in Key Resources Table. Samples were incubated with antibodies O/N at 4°C. 25 μL of FA(1) buffer washed Dynabeads were added to each sample and they were incubated for 2 hours at 4°C. Samples were then washed 3x for 5 min at RT with FA(1) buffer, FA(2) buffer (FA(1) buffer with 500 mM NaCl), once with LiCl buffer (10 mM TrisHCl, pH 8.0, 0.25 M LiCl, 1 mM EDTA, 0,5% NP-40 (v/v), 0,5% NaDeoxycholate (w/v)) and once with TE buffer. DNA was eluted from the antibodies with ChIP Elution buffer (50 mM Tris HCl, pH 7.5, 10 mM EDTA, 1% SDS) for 15 min at 65°C in a thermomixer set to 1300 rpm. DNA was treated with Proteinase K and de-crosslinked O/N at 65°C. DNA was purified with Zymo Research ChIP DNA Clean and Concentrator kit according to the manual instructions. To obtain enough material for the library preparation usually 3 technical IP replicates were pulled. The ChIP-seq libraries were prepared with 2 ng of DNA with NEBNext®Ultra II DNA Library Prep Kit for Illumina® according to the manual instructions. The libraries were barcoded and sequenced at LAFUGA at the Gene Center (LMU). For ChIP-QPCR, the isolated DNA was quantified by qPCR as described for the gene expression analysis. Unless otherwise noted, the mean was calculated from three independent experiments and errors bars were calculated as SEM and displayed accordingly. QPCR signals were normalized against the input samples for each primer position as internal control. For ChIP experiments with anti-H3K9me2, anti-Swi6, anti-H3K9me3, the input normalized values were corrected for variation in IP efficiency by normalizing against the mean of 3 euchromatin loci (act1, adh1-prom, adh1-5prime). For RNAPII Ser2P ChIP, the input normalized values were corrected for variation in IP efficiency by normalizing against the mean of 3 euchromatin loci (act1, ade2, adh1-3prime). Euchromatin normalized ChIPs were displayed as 'Norm to EU'. For ChIP experiments with anti-Pob3, anti-Spt16 and anti-HA (Clr4-HA ChIP) ChIP signals were normalized to input and displayed as '% of Input'. For the histone turnover ChIP, incorporation of the new histone H3-T7 was calculated as follows: input normalized signals from the β-estradiol-uninduced samples were subtracted from the input normalized signals from the β-estradiol-induced samples as displayed as '4hrs-0hrs' HU.

ChIP-seq analysis

Single-end reads (50 bp) were mapped to the reference genome (*Schizosaccharomyces pombe* ASM294v2) using bowtie2 (version 2.2.9). Reads were counted in either 250 bp or 10 kb windows (bins) using the windowCounts() function from the csaw R/Bioconductor package (version 1.18.0). Normalization factors were calculated by the normFactors() function using the "TMM" method on count matrices with 10 kb bins and applied on count matrices with 250 bp bins. Normalized, log2-transformed count matrices were obtained by the cpm() function (edgeR package, version 3.26.8). ChIP samples were normalized by their corresponding inputs (i.e., subtraction in log2-scale). Input-normalized count matrices were converted to coverage vectors using the coverage() function (GenomicRanges package, version 1.38.0) and exported as bigwig files (rtracklayer package, version 1.44.4). For visualization, coverages were smoothed by the rollmean() function (zoo package, version 1.8.9) and plotted using custom R functions.

Broad H3K9me2 peaks were identified using the Homer software package (Heinz et al., 2010). Tag directories were created with the settings -mapq 1 and parameters for findPeaks command were set to -style histone -F 2. Peaks were called on replicates independently and the intersect was taken as final set.

Normalized count matrices (with 250 bp bins) were subset by telomeric, centromeric heterochromatin or euchromatin regions on chromosome I and II. Telomeric and centromeric bins were selected by the overlap of wild-type H3K9me2 peaks with telomeres (I:1-100000; I:5479000-5579000; II:1-100000; II:4440000-4539000) or centromeres (I:3720000-3820000; II:1570000-1670000), respectively. The data were aggregated using two approaches: either replicates were averaged and values of bins were visualized as boxplots or the median of bins were calculated for each replicate and region, and visualized as dot plots. Statistical analysis was performed on aggregated data using the second approach (i.e., on medians). P values were obtained by fitting a linear mixed effect model (lme4,_version 1.1-27 and lmerTest, version 3.1-3 packages) with genotype (e.g., wild-type or *pob3Δ*) and region (e.g., telomeric, centromeric or euchromatin) as fixed effects and sample id as random intercept.

Histone turnover assay

RITE histone turnover assay was done as before (Greenstein et al., 2018) with several modifications. Briefly, cells were inoculated from a pre-culture to 100 mL YES supplemented with Hygromycin B (100 μg/ mL, Invitrogen) and grown O/N at 30°C to OD600 0.4-0.8. 20 ODs of cells were taken and processed for ChIP as the 0 hr (uninduced) time point. The remaining cells were washed 2x in media devoid of Hygromycin B. 12.5 ODs of cells were taken and resuspended in 50ml YES supplemented with 15 mM Hydroxyurea (HU) and 1.5 μM

β-Estradiol (ER) and incubated further for 4 additional hours at 30°C. 20 ODs of cells were processed for ChIP as the 4 hr (induced) time point.

Protein extract preparation

Whole cell extracts (WCE) were prepared as published before (Murawska et al., 2020). Briefly, 50 mL yeast cultures were grown to mid-log phase (OD600 0.5-0.8). The cultures were spun down and cell pellets were resuspended in 500 μL of Workman Extract Buffer (40mM HEPEs pH7.4, 250mM NaCl, 0.1% NP40, 10% Glycerol, 1 mM PMSF, Roche proteinase inhibitors). 250 μL of glass beads were added and cells were lysed with Peqlab precellys homogenizator (3x30 s). The extracts were shortly spun down at 2500 rpm at 4°C. The supernatant and the pellet were treated with benzonase in the presence of 2mM MgCl2 for 30 min on ice and spun down at the maximum speed for 10 min at 4°C. The extracts were frozen in liquid nitrogen and stored at −80°C or immediately used for western blot analysis. Protein concentration was measured with Bradford reagent (BioRad).

For HU treatment assay, strains were pre-cultured in liquid YES at 27°C for 24 hours, back diluted and grown to log-phase. A control (untreated) culture and treated culture (20mM HU) were incubated for a further 2 hours at 27°C. Total protein extracts from OD600 = 1 were prepared by trichloroacetic acid (TCA) precipitation according to (Knop et al., 1999). Proteins solubilized in HU buffer (200 mM phosphate buffer, pH 6.8, 8 M urea, 5% w/v SDS, 1 mM EDTA,100 mM DTT) and heat denatured at 65°C for 10 minutes were separated with SDS-polyacrylamide gel electrophoresis and subjected to Western Blot analysis.

Western blot

Western blot was performed as published before (Murawska et al., 2020). Briefly, proteins were separated with SDS-polyacrylamide gel electrophoresis and electroblotted onto methanol activated polyvinylidene difluoride (PVDF) membranes in Blotting Buffer (20 mM Tris, 192 mM glycin, 20% methanol) for 1hr at 400 mA at 4°C. Membranes were then incubated in Blocking Buffer (TBS, 0.1% Tween 20, 5% non-fat dry milk) for 40 min - 1hr at RT followed by an incubation in the Blocking Buffer with the appropriate primary antibody for 1hr at RT. Membranes were washed three times for 5 min in Washing Buffer - TBST (TBS, 0.1% Tween 20) and then incubated in Blocking Buffer containing the appropriate fluorescence or HRP-conjugated secondary antibodies for 40 min - 1 hour at RT followed by 3 times washing in TBST for 5-10 min. Fluorescent western blot signals were visualized with Li-Cor Imaging System. Chemiluminescent western blot signals were visualized with the Immobilon Western Chemiluminescence HRP substrate (Millipore, WBKLS0500) using BioRad ChemicDoc MP Imaging System.

HSS assay

Cells containing HSS reporters were grown for flow cytometry experiments as described (Greenstein et al., 2020). Flow cytometry was performed using a Fortessa X20 dual machine (Becton Dickinson) and high-throughput sampler (HTS) module. Depending on strain growth and sample volume, data from approximately 4,000–100,000 cells were collected. Fluorescence detection, compensation, and data analysis were done as described (Al-Sady et al., 2016; Greenstein et al., 2018). 2D-density histogram plots were generated as described previously (Greenstein et al., 2018) with the following exceptions: Data from biological replicates were merged together prior to plotting. Hexbin plots were generated in R via the ggplot2 package. The guide-lines for cutoff values of "off" and "on" states for Green and Orange were determined using mean of a Red-Only control strain plus 3 times the standard deviation (SD) and mean of *clr4Δ* (after removal of color-negative cells) minus 1 SD value respectively. For the *spt16-1* experiment, the fraction of cells below the "off" threshold for both "green" and "orange" were calculated for each biological replicate independently.

Cell cycle analysis

PAS99 wild-type, *pob3Δ::KAN* and *spt16-1:KAN* cells were struck onto YS plates, and grown at 27°C in EMM liquid culture. Cell were diluted to OD 0.1 and grown another 9 hr in EMM at 27°C till OD ~0.5-0.8. For the *cdc25* experiment, cells were grown at 25°C overnight, diluted as above and then either kept at 25°C or moved to 37°C for 2 or 4hrs. Cells were then fixed, RNaseA treated and stained with Sytox Green as described (Knutsen et al., 2011) but instead of sonication, cells were vigorously vortexed just prior to Flow cytometry analysis. Flow cytometry and analysis was performed as described (Greenstein et al., 2018). Within each experiment, the same gates were applied to all specimen for forward and side scatter, to select a population of similar sized and shaped cells to analyze, and for Width and Area of SyTOX green fluorescence, to assess cell cycle stage distributions.

QUANTIFICATION AND STATISTICAL ANALYSIS

Quantification, number of replicates and statistical tests employed are described in the figure legends or in the method section. Shortly, for RT-QPCR, RITE assay and RNAPII ChIP-QPCR statistical analysis was done on log2 transformed values. One-way ANOVA was performed, and different letters were assigned with significant differences with a Tukey's post hoc test at $p < 0.05$. For ChIP-QPCR data at Figures 4A, 4B, and 4D statistical analysis was performed by fitting a linear mixed effect model (R packages: lme4 version 1.1-27 and lmerTest version 3.1-3), where the group variable (i.e., the combination of primer and genotype) served as a fixed effect and the sample variable (i.e., the combination of replicate number and genotype) as a random intercept. For each primer, mutant versus wild-type comparisons were tested and p values were adjusted by the Benjamini-Hochberg method. The details of statistical analysis can be found in the figure legends, p values are listed in Table S3.